Ultrasmall Gold Nanoparticles Anchored to Graphene and Enhanced Photothermal Effects by Laser Irradiation of Gold Nanostructures in Graphene Oxide Solutions

Abdallah F. Zedan, Sherif Moussa, James Terner, Garrett Atkinson, and M. Samy El-Shall[†,*]

Department of Chemistry, Virginia Commonwealth University, Richmond, Virginia 23284, United States and [†]Department of Chemistry, King Abdulaziz University, Jeddah, Saudi Arabia

ABSTRACT In this work we demonstrate the coupling of the photothermal effects of gold nanostructures of controlled size and shape with graphene oxide nanosheets dispersed in water. The enhanced photothermal effects can be tuned by controlling the shape and size of the gold nanostructures, which result in a remarkable increase in the heating efficiency of the laser-induced size reduction of gold nanostructures. The Raman spectra of the Au—graphene nanosheets provide direct evidence for the presence of more structural defects in the graphene lattice induced by laser irradiation of graphene oxide nanosheets in the presence of Au nanostructures. The large surface areas of the laser-reduced graphene oxide nanosheets with multiple defect sites and vacancies provide efficient nucleation sites for the ultrasmall gold nanoparticles with diameters of 2—4 nm to be anchored to the graphene surface. This defect filling mechanism decreases the mobility of the ultrasmall gold nanoparticles and, thus, stabilizes the particles against the Ostwald ripening process, which leads to a broad size distribution of the laser-size-reduced gold nanoparticles. The Au nanostructures/graphene oxide solutions and the ultrasmall gold—graphene nanocomposites are proposed as promising materials for photothermal therapy and for the efficient conversion of solar energy into usable heat for a variety of thermal, thermochemical, and thermomechanical applications.

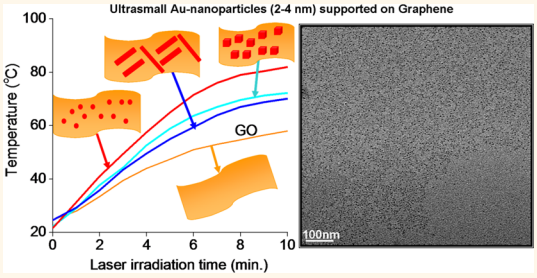

KEYWORDS: graphene oxide · shape-controlled gold nanostructures · photothermal energy conversion · laser-induced size reduction · surface plasmon resonance · graphene defects · Raman spectra of gold—graphene nanocomposites

Gold nanostructures have a remarkable capacity to absorb and scatter light over a broad range of the visible and near-infrared regions, depending on the particles' size and shape.[1−4] These interactions also trigger photothermal effects where electronic oscillations at the particle surface are converted to heat, which raises the particles' temperature, as determined by the surface plasmon resonance (SPR).[1,2,5−7] These phenomena have been extensively investigated for a variety of applications in biomedical imaging,[2,7−9] cancer therapy and diagnosis,[7,10,11] catalysis,[12] sensors,[13] and photonic devices.[14]

In addition to gold nanoparticles, photothermal energy conversion by carbon nanotubes (CNTs) has been also extensively studied mostly for photothermal therapy applications.[15−18] Most recently, interest has been focused on graphene and graphene oxide (GO),[19−21] which have recently emerged as novel nanocarbon materials with potential uses in energy applications, including photothermal energy conversion, in addition to nanoelectronics, supercapacitors, batteries, photovoltaics, and related devices.[22,23] The large surface area (2600 m^2g^{-1}) of graphene and the strong optical absorption across the spectrum (2.5% of the white light) coupled with its high thermal and chemical stability can lead to a rapid temperature rise and subsequent energy transfer to the host medium, thus, offering an efficient way of heating the medium.[22,23] This has been recently demonstrated by the development of a facile

* Address correspondence to mselshal@vcu.edu.

Received for review October 15, 2012 and accepted November 29, 2012.

Published online November 29, 2012
10.1021/nn304775h

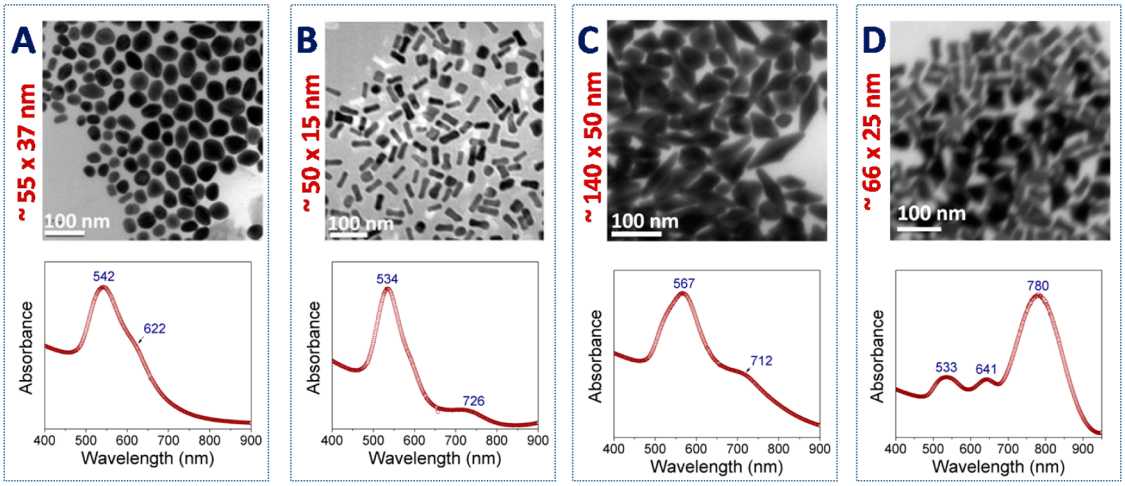

Figure 1. TEM images and UV−vis absorption spectra of Au nanostructures with different shapes: (A) spheroids, hexagonal plates, (B) SRs, (C) bipyramids, and (D) dog bones.

laser reduction method for the synthesis of laser converted graphene (LCG), which provides a solution processable synthesis of individual graphene sheets.[24,25] In this process, irradiation of GO suspended in water using the second or the third harmonic of a Nd:YAG laser (532 or 355 nm, respectively) results in significant deoxygenation of GO and the formation of LCG. This remarkable photothermal conversion of energy results in a significant temperature rise of water from room temperature to 75 °C in a few minutes of laser irradiation (532 nm of nanosecond pulses at 30 Hz with an average power of 6 W).[24]

The interaction of gold nanoparticles with pulsed laser light tuned to the SPR bands of the gold nanostructures can result in a sequence of heating, melting, and evaporation processes that could lead, in addition to the photothermal energy effects, to significant size reduction of the original gold nanoparticles.[26−31] The coupling of the SPR of gold nanostructures with the photothermal effects of GO could enhance the melting and evaporation of the Au nanostructures and the formation of ultrasmall Au nanoparticles attached to the large surface area of the laser converted graphene sheets. Herein, we report on the enhanced photothermal energy conversion by gold nanoparticles of well-defined size and shape dispersed in GO solutions as efficient photothermal materials for a variety of applications involving rapid heating of water. Furthermore, we demonstrate that the enhanced photothermal energy conversion by the gold−GO aqueous solutions can be tuned by controlling the shape of the Au nanostructures from spherical particles to short and long nanorods. We also report the synthesis of ultrasmall gold nanoparticles with diameters of 2−4 nm well-dispersed on the laser converted graphene nanosheets. The coupling of the laser-induced size reduction of the gold nanoparticles with the laser conversion of graphene oxide into graphene (LCG) provides a novel method for the synthesis of ultrasmall gold nanoparticles from much larger particles with different sizes and shapes. These ultrasmall gold−graphene nanocomposites are proposed as novel photothermal energy convertors for a variety of thermochemical and thermomechanical applications, in addition to photothermal therapy, such as heating and evaporation of liquids by solar energy, ignition of solid fuels, and welding of composite materials.

RESULTS AND DISCUSSION

Size and Shape Effects of Gold Plasmon Absorbance. Figures 1 and 2 display TEM images and UV−vis absorption spectra of the as-prepared shape-controlled Au nanostructures using the seed-mediated growth method,[32−34] with some modifications. These modifications (see Experimental Section) allow fine-tuning and morphological control of the Au nanostructures by systematically varying the concentration of the silver ions in the growth solution. By increasing the concentration of the Ag ions in the growth solution, gold nanostructures with well-defined shapes of spheroids (hexagonal plates), short rods (SRs), bipyramids, dog bones, long rods (LRs), round-corner rectangular plates, sharp-corner rectangular plates, and cubes can be prepared as shown in Figures 1A−D and 2A−D, respectively. Different mechanisms have been proposed to explain the shape-controlled synthesis of gold nanostructures, but most of the mechanisms are based on the selective adsorption of surfactant and accordingly blocking the growth at specific crystallographic faces.[32−36]

The evolution of the SPR bands of the Au nanostructures with the shape changes is clearly evident in the UV−vis absorption spectra shown in Figures 1 and 2. The results show the same trends reported in the literature where no SPR is observed for ultrasmall Au nanoparticles with 2−4 nm diameters[37] (seed particles, Figure S1, Supporting Information, SI) and a single

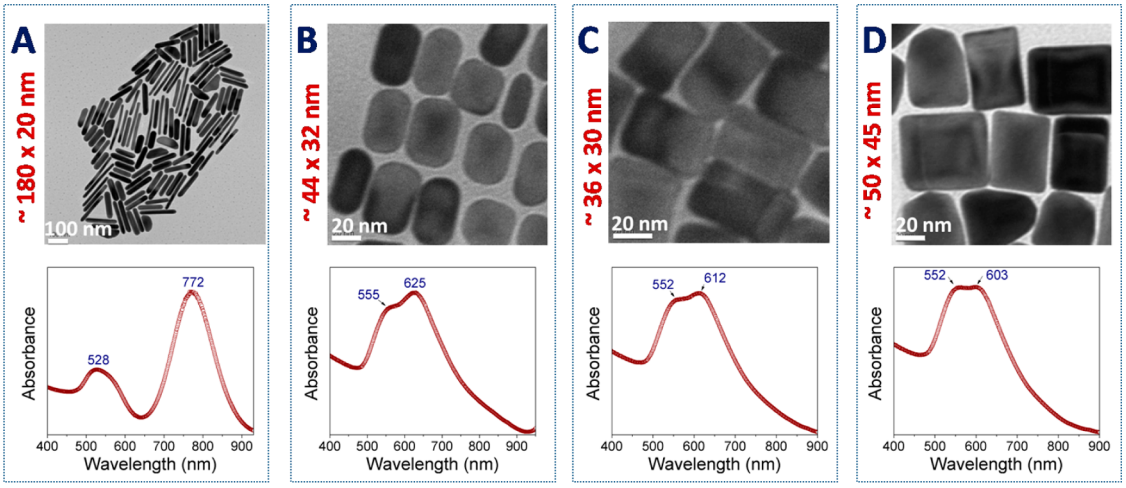

Figure 2. TEM images and UV−vis absorption spectra of Au nanostructures with different shapes: (A) LRs, (B) round-corner rectangular plates, (C) sharp-corner rectangular plates, and (D) cubes.

band around 520−530 nm, weakly dependent on the particle size, is observed for spherical particles (Figure S2, SI).[32−36] Gold LRs (Figure 2A) exhibit two SPR bands, near 528 and 772 nm, due to the transverse and the longitudinal electronic oscillations, respectively.[5,33−36] Gold nanoparticles with prism or quasi-prism shapes have three SPR bands due to the in-plane dipole plasmon resonance, the in-plane quadrupole resonance, and the out-of-plane quadrupole resonance (Figure 1C,D).[5,33−36] The out-of-plane dipole resonance is sufficiently weak and broad that it is barely discernible as a shoulder on the in-plane resonance (Figure 1C). The in-plane dipole plasmon resonance is very sensitive to the sharpness of the tips on the triangles.[5,33−36] These unique optical properties of anisotropic gold nanocrystals enable the tuning of SPR to any wavelength specific to a particular application from the visible to the NIR spectral regions.[3,4,7]

We selected six distinct shapes of the gold nanostructures, namely, spheroids (Figure 1A), SRs (Figure 1B), bipyramids (Figure 1C), LRs (Figure 2A), and cubes (Figure 2D), in addition to the small spheres prepared by a citrate reduction method[38] (Figure S2, SI) to investigate the photothermal energy effects and laser-induced size reduction of the gold nanostructures in the absence and presence of GO. For each selected shape, two solutions containing similar concentrations of Au nanoparticles of the same shape with and without GO were laser-irradiated under identical conditions. Absorption spectra and TEM images were recorded for each solution before and after the laser irradiation. The temperature rise of each solution was also monitored during the laser irradiation. The results are presented in Figures 3−5 and are discussed below.

Laser-Induced Size Reduction of Gold Nanostructures. Figure 3A and 3B display TEM images of the spherical Au nanoparticles after the 532 nm laser irradiation in the absence and presence of GO, respectively (TEM images of the as prepared spherical particles are shown in Figure S2, SI). The TEM image shown in Figure 3A indicates a slight decease in the average size of the spherical particles from 13 ± 2 to 10 ± 2 nm following the laser irradiation in water. The corresponding SPR band exhibits a small blue shift from 532 to 512 nm, as shown in Figure 3C, consistent with the weak dependence of the SPR of spherical Au nanoparticles on particle size.[5,35,36] In the presence of GO, the 532 laser irradiation results in the almost disappearance of the SPR band, as shown in Figure 3C, suggesting more effective evaporation of the Au nanoparticles during the laser irradiation of the Au−GO solution. This, indeed, is confirmed by the TEM image shown in Figure 3B, which indicates that the diameters of the Au nanoparticles are significantly decreased from 13 ± 2 to 5.4 nm upon laser irradiation in the presence of GO. Thus, both the absorption spectra and the TEM micrographs clearly show that, after the 532 nm laser irradiation in the presence of GO, the Au nanoparticle sizes become profoundly smaller than in the absence of GO under identical laser irradiation conditions. This result implies that the temperature of gold nanoparticles during the laser irradiation is much higher in the presence of GO than in pure water. This is consistent with the measured temperature changes caused by laser irradiation of the laser three solutions of spherical Au nanoparticles in water; GO in water and spherical Au nanoparticles dispersed in a GO−water mixture under identical experimental conditions, as shown in Figure 3D. The temperature of the GO solution containing spherical Au nanoparticles reaches 69 °C after 10 min of laser irradiation (532 nm, 4 W, 30 Hz) in comparison with the same concentration of spherical Au nanoparticles in water and the GO solution without Au nanoparticles, which reach 47 and 56 °C, respectively, under identical experimental conditions. The higher temperature rise observed for the Au nanoparticles dispersed in the GO

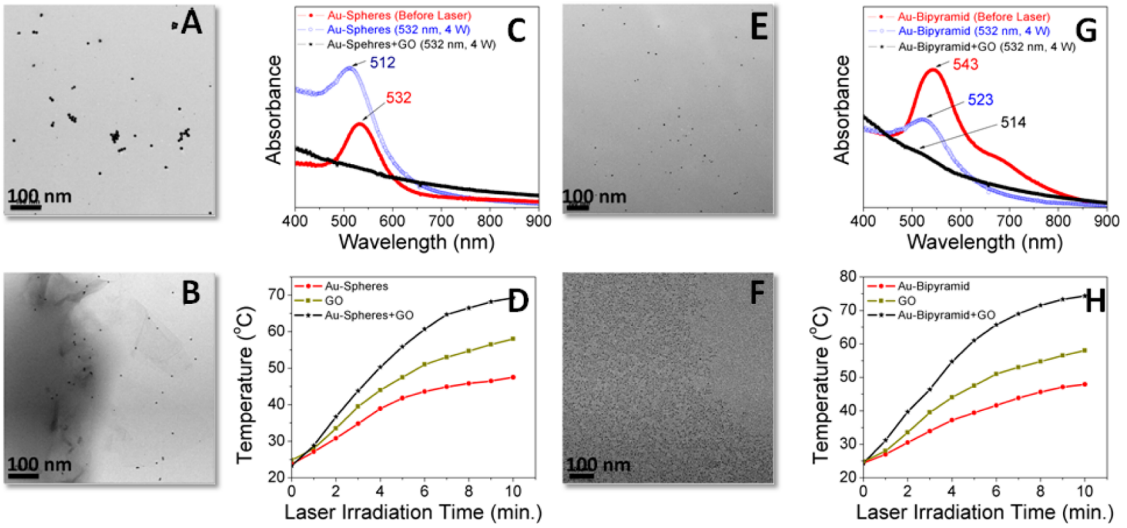

Figure 3. TEM images of spherical Au nanoparticles after the 532 nm laser irradiation in the absence (A) and presence of GO (B) and bipyramidal Au nanoparticles after the 532 nm laser irradiation in the absence (E) and presence of GO (F). UV−vis absorption spectra of the Au nanoparticles after laser irradiation in water (blue) and in GO (black) are shown for the spherical and bipyramidal particles in (C) and (G), respectively. Temperature profiles showing the increase of the solutions' temperatures are shown for the spherical and bipyramidal particles in (D) and (H), respectively.

solution demonstrates that the coupling of the photothermal effects of Au nanoparticles and GO can result in highly efficient photothermal energy convertors. The temperature rise during the irradiation of the Au nanoparticles−GO solution assists in anchoring the nanoparticles to the defect sites created by the laser reduction of GO, thus, resulting in uniform dispersion of the small Au particles among the reduced GO nanosheets, as shown by the TEM image of Figure 3B.

Figure 3E, 3F and 3G display TEM images and UV−vis absorption spectra of the as-prepared bipyramidal Au nanoparticles after the 532 nm laser irradiation in the absence (E) and presence (F) of GO. The absorption spectra of the as-prepared bipyramidal nanoparticles (Figure 1C) show two absorption bands at 567 and 712 nm corresponding to the transverse and the longitudinal SPR bands. Both bands disappear following the laser irradiation in water, as shown in Figure 3G, with the appearance of one SPR band at 523 nm indicating the melting of the Au-bipyramidal nanoparticles and the reforming of Au nanospheres during the laser irradiation process. This is confirmed by the TEM image displayed in Figure 3E, which shows spherical particles with an average size of 4.3 $\pm$ 1.5 nm as compared to the dimensions of the original bipyramidal particles of 140 $\times$ 50 nm (shown in Figure 1C). Interestingly, the same laser irradiation in the presence of GO converts the bipyramidal particles into ultrasmall spherical particles with an average diameter of 1.6 $\pm$ 0.6 nm, as shown in Figure 3F. This size reduction is accompanied by a rapid increase in solution temperature reaching about 74 °C in 10 min of laser irradiation, as shown in Figure 3H. This increase in temperature reflects the net heat transfer to water, resulting from the coupled photothermal effects of the Au bipyramidal nanoparticles and GO.

Figures 4A, 4B and 4C display TEM images and UV−vis absorption spectra of the as-prepared Au SRs after the 532 nm laser irradiation in the absence (A) and presence (B) of GO. The as-prepared Au SRs are characterized by average dimensions of 50 $\pm$ 5 $\times$ 15 $\pm$ 2 nm (aspect ratio ~3.3) and exhibit two SPR bands at 534 and 726 nm, as shown in Figure 1B. Following the laser irradiation in the absence of GO, only the transverse band around 520 nm is observed in the absorption spectrum, as shown in Figure 4C, consistent with the formation of small spherical nanoparticles with average diameters of 5.3 $\pm$ 1.9 nm, as evident from the TEM image in Figure 4A. However, the Au nanoparticles formed following the laser irradiation of the particles dispersed in the GO solution have an average diameter of 2.4 $\pm$ 0.55 nm, as shown in Figure 4B, consistent with the near disappearance of the SPR band except for a small shoulder at 517 nm, as shown in Figure 4C. The formation of these ultrasmall Au nanoparticles is accompanied by a strong enhancement in the photothermal energy conversion of the Au SRs dispersed in the GO solution where the solution temperature reaches 70 °C after 10 min of laser irradiation (532 nm, 4 W, 30 Hz) as compared to 47 and 56 °C for the Au SRs in water and the GO solution, respectively, under identical experimental conditions, as shown in Figure 4D.

The as-prepared Au LRs have an average length and width of 180 $\pm$ 20 and 20 $\pm$ 5 nm, respectively (aspect ratio ~ 9), and exhibit two SPR bands, the transverse near 528 nm and the longitudinal near 772 nm (Figure 2A). Following the 532 nm laser irradiation, the longitudinal band disappears and the transverse band shifts to 523 nm (Figure 4G), indicating the transformation of the Au LRs into smaller spherical particles. This is clearly shown in the TEM image shown

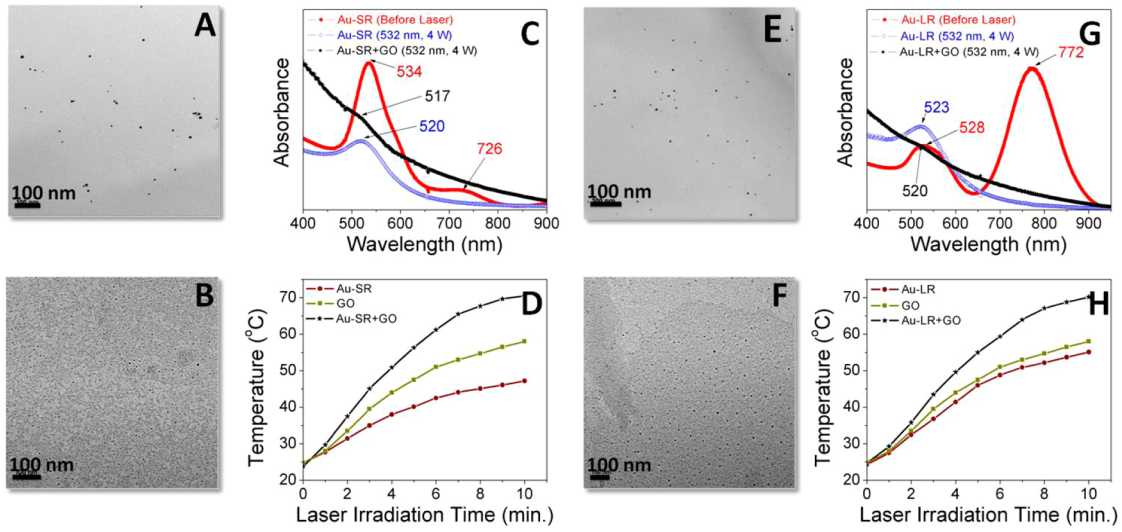

Figure 4. TEM images of the Au SRs after the 532 nm laser irradiation in the absence (A) and presence of GO (B) and the Au LRs after the 532 nm laser irradiation in the absence (E) and presence of GO (F). UV−vis absorption spectra of the Au nanoparticles after laser irradiation in water (blue) and in GO (black) are shown for the SRs and LRs in (C) and (G), respectively. Temperature profiles showing the increase of the solutions' temperatures are shown for the SRs and LRs in (D) and (H), respectively.

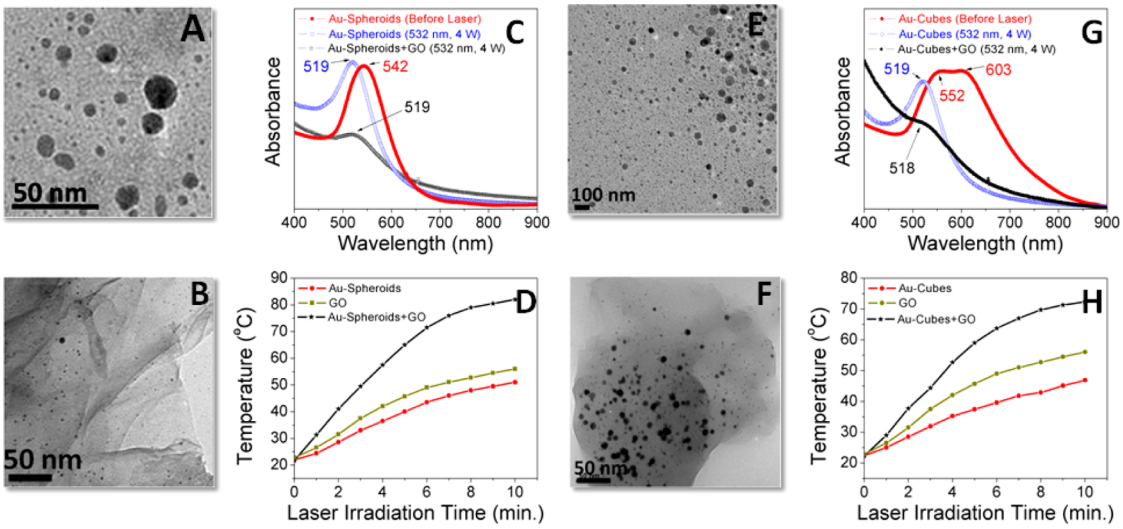

Figure 5. TEM images of the Au spheroids after the 532 nm laser irradiation in the absence (A) and presence of GO (B) and the Au cubes after the 532 nm laser irradiation in the absence (E) and presence of GO (F). UV−vis absorption spectra of the Au nanoparticles after laser irradiation in water (blue) and in GO (black) are shown for the Au spheroids and cubes in (C) and (G), respectively. Temperature profiles showing the increase of the solutions' temperatures are shown for the spheroids and cubes in (D) and (H), respectively.

in Figure 4E, where spherical particles with an average diameter of 5.5 ± 1.9 nm are observed. Again, laser irradiation of the Au LRs in the presence of GO results in well-dispersed ultrasmall Au nanoparticles with an average diameter of 2.9 ± 1.7 nm, as shown in Figure 4F. Accordingly, the transverse SPR band almost disappears following the laser irradiation of the Au LRs in GO, as shown in Figure 4G. The measured temperature change caused by laser irradiation of the Au LRs in the GO solution indicates that the solution temperature reaches 70 °C after 10 min of laser irradiation (532 nm, 4 W, 30 Hz), as compared to 55 and 56 °C for the Au LRs in water and GO solution, respectively, under identical experimental conditions, as shown in Figure 4H. Again, similar to the Au spherical and SR particles, the presence of GO results in a significant enhancement in the observed photothermal effects.

The results for the Au spheroids (shown in Figure 5A−D) and Au cubes (shown in Figure 5E−H) follow the same general trends observed for the other Au shapes, thus, leading to generalized findings. Typically, laser irradiation in the presence of GO results in smaller spherical Au nanoparticles well-dispersed on the reduced GO nanosheets accompanied by a strong enhancement in the photothermal effect, as is evident by the significant increase in the temperature of the

Au–GO solution, as compared to the individual Au and GO solutions. However, the size reduction of the Au spheroids and cubes is not as much as with the other shapes (spherical, bipyramids, SRs, and LRs) where ultrasmall Au nanoparticles with no SPR peaks[37] were observed following the laser irradiation of the Au particles in the presence of GO (Figure S3, SI). This appears to be related to the volume of the particles where the large volumes of the spheroids and cubes may require longer irradiation times and higher laser powers in order to effectively melt and vaporize the large Au nanoparticles.[26] The melting of the nanoparticles leads to the shape change from nonspherical to spherical particles and the size reduction is due to the vaporization of the particles. According to the theoretical estimation and experimental results of Pyatenko *et al.*,[30] under low laser energy flow density (less than 10^{12} W/m^2 similar to the conditions of the current experiments), the particle heating–melting–evaporation mechanism is solely responsible for the size reduction of the nanoparticles.

Enhanced Photothermal Energy Conversion. The observed temperature rise reflects the steady state net heat transfer from Au nanoparticles and RGO nanosheets to the solution. Figure 6 compares the extent of temperature rise for different shapes of Au nanostructures in the absence and presence of GO. Table S1 (SI) lists the maximum temperature rise observed for different shapes of Au nanoparticles following the 532 nm laser irradiation in the presence and absence of GO under identical experimental conditions.

Both GO and gold nanostructures show significant photothermal effects. When exposed to the 532 nm YAG laser (4 W, 30 Hz), the GO solution containing spheroid Au particles displays the highest temperature rise (58 °C above the temperature of 24 °C of the nonexposed solution) followed by the GO solutions containing the Au cubes (48–53 °C), then the Au bipyramids and dog bones (50–51) °C), then the Au long and SRs (46 °C), and finally the small Au spheres (45 °C). The observed trend appears to be related again to the volume of the particles and the melting temperatures of different shape nanostructures. For example, the larger volume of the hexagonal plates (spheroids) and probably their lower melting temperature result in more heat being transferred to water and, thus, a rise in the temperature of the solution by 58 °C. Similarly, the large volumes of the nanocubes result in a significant temperature rise of water (53 °C). For comparison, the smaller volumes of the small spherical Au particles (Figure 3A) result in weaker photothermal effect and consequently less temperature rise of water (45 °C). For the Au nanorods, both the small volumes and probably the higher melting temperatures result in less heat transferred to the solution and consequently a temperature rise of about 46 °C as compared to 58 °C for the hexagonal plates.

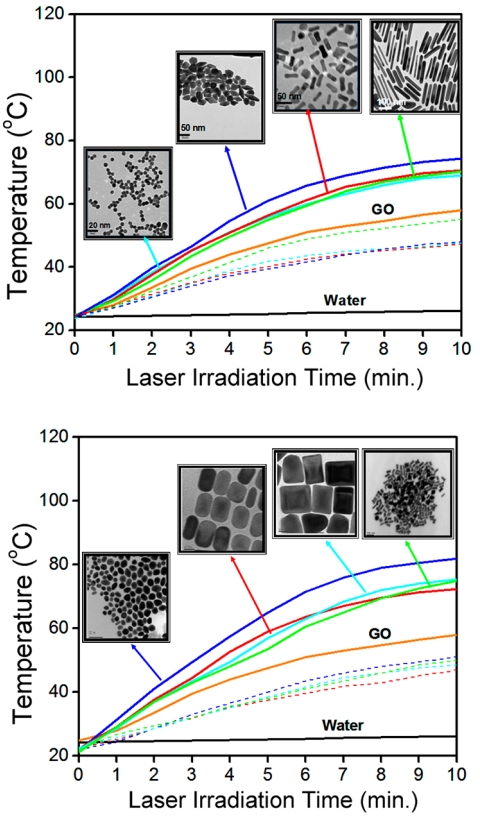

Figure 6. Temperature profiles during the 532 nm laser irradiation (4 W, 30 Hz) of preformed Au nanostructures in aqueous solutions in the presence (solid lines) and absence (dashed lines) of GO.

In contrast to the Au–GO solutions, the temperature changes of the Au and GO individual solutions are less significant under the same laser irradiation conditions. For example, the GO solution without Au nanoparticles shows only a 32 °C of temperature rise within 10 min of laser irradiation. Similarly, the temperature rise of the Au nanoparticles in water ranges from 23 °C for the spherical particles to 27 °C for the hexagonal (spheroid) particles under the same concentration and laser irradiation conditions. These results clearly demonstrate that the Au–GO solutions have better photothermal effects than individual Au nanostructures and GO solutions. Therefore, it is clear that the coupling of the surface plasmon resonance of gold nanoparticles with the laser reduction of graphene oxide leads to significant enhancement of the efficiency of photothermal energy conversion by the gold nanoparticles–graphene oxide mixtures. The enhanced photothermal effects can be tuned by controlling the shape and size of the gold nanostructures, which result in a remarkable increase in the heating efficiency of the laser-induced size reduction of gold nanostructures.

A number of recent studies have shown the promise of using graphene oxide-based composites in various areas of biomedicine such as cancer therapy and

imaging, drug delivery, and biomodulation.[19−21,39−43] It has been found that functionalized reduced GO sheets are potentially stable in physiological environments and are nontoxic to cells in mice *in vivo*.[20] The efficient photothermal energy conversion of the Au nanostructures−GO solutions reported here may provide great opportunities for cancer treatment. For example, the observed temperature rise of the laser irradiated Au−GO solutions is significantly higher than that observed for the SWNT-Au-PEG nanocomposites, which have shown high photothermal cancer cell killing efficacy.[44] Irradiation of the SWNT-Au-PEG solution with the 808 nm NIR laser at a power density of 1 W/cm^2 showed nearly a 30 °C of temperature rise within 5 min.[44] In contrast, irradiation of the current Au spheroids−GO solution with the 532 nm laser (4 W, 30 Hz) for 5 min causes a temperature rise of nearly 40 °C. Therefore, it is expected that the current Au nanostructures−GO solutions would exhibit improved photothermal cancer cell killing efficacy due to the strong photothermal energy conversion contributed by the gold nanostructure and GO. However, substantial work remains to be done in order to fine-tune the surface chemistry of the Au−GO nanocomposites to optimize their uptake and nontoxicity behaviors for *in vitro* or *in vivo* biomedical applications. The strong light absorbing capabilities of Au nanostructures in the NIR region are expected to dramatically increase if the Au−GO nanocomposites are properly functionalized. For example, the integration of GO with Au nanostructures has been shown to significantly enhance the two-photon excitation processes and a 4-fold enhancement factor was observed for the Au−GO nanocomposites compared to pure Au nanostructures.[45] Experiments to investigate the effect of polymer coating on the *in vitro* behaviors of the Au−GO nanocomposites, their physiological stability, and cellular uptake are currently under way in our laboratory.

Correlation between Raman Spectra and Defect Sites in Laser-Converted Graphene. Our results clearly indicate that the presence of GO enhances the heating efficiency of the Au nanostructures following the absorption of the 532 nm photons, which leads to the subsequent melting and evaporation processes, resulting in the formation of monodisperse ultrasmall Au nanoparticles supported on the LCG nanosheets. Previous work has demonstrated that the 532 nm laser irradiation of the Au nanoparticles resulted in a significant size reduction from an initial diameter of 54 ± 7 nm to an average diameter of 6 nm but with a bimodal size distribution.[31] The bimodal size distribution is attributed to the Ostwald ripening process where the initially formed small particles with higher surface energies are consumed in the growth of the large particles with lower surface energies at longer irradiation times.[31] The absence of bimodal size distributions in the Au nanoparticles formed by laser irradiation in the presence of GO in the present work suggests that the mobility of the particles is

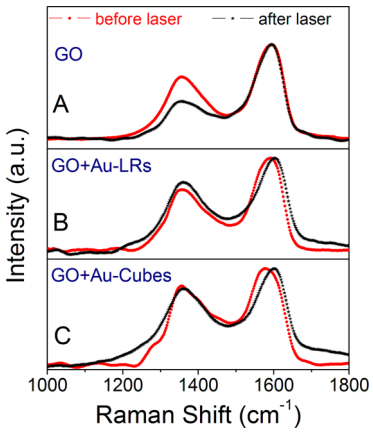

Figure 7. Raman spectra of GO (A), GO + Au nanorods (B), and GO + Au nanocubes (C) before (red) and after (black) laser irradiation for 10 min (532 nm, 4 W, 30 Hz) in solution.

significantly reduced to a degree that does not allow for the dynamic Ostwald ripening process.[46] This can be explained if the small Au particles are anchored to defect sites on the reduced GO nanosheets that can restrict their mobility. It is now well established that both the chemical and the laser reduction of GO result in the formation of graphene nanosheets with a significant number of defect sites including vacancies, disorder, defective edges, and many others.[47−54] In the laser converted graphene, the nature of these defects depends on the oxygen functional groups interacting with the photogenerated electrons and holes within GO.[50,53,54]

Raman spectroscopy is one of the most useful techniques that can identify the nature of defects and disorder in the graphene and Au−graphene nanosheets.[55−58] To gain information on the extent of defects in the Au−graphene nanosheets, we have applied Raman spectroscopy to compare the LCG with the graphene-containing Au nanoparticles both formed by laser irradiation of GO. Figure 7A compares the Raman spectra of GO before and after the 532 nm laser irradiation (10 min, 4 W, 30 Hz). The spectrum of the exfoliated GO exhibits the characteristic G-band (1594 cm^{-1}) and the D-band (1354 cm^{-1}) with a D/G intensity ratio of about 0.70. The G-band arises from the vibration of the sp^2-bonded carbon atoms and the D-band is attributed to structural disorder at defect sites with the D/G ratio usually taken as a measure of the quality of the graphitic structures, because for highly ordered pyrolitic graphite, this ratio approaches zero.[55−57] Following the 532 nm laser irradiation of GO, the D/G ratio decreases to 0.40, indicating a significant reduction of the degree of disorder and defect sites in the LCG. However, no decrease in the intensity of the D-band relative to the G-band is observed following the laser irradiation of the GO−Au nanoparticle solutions, as shown in Figure 7B,C for the Au LRs and cubes, respectively. In fact, the D/G ratio increases to 0.8 (higher than the D/G ratio of GO) after the laser

irradiation of the GO solutions containing either the Au nanorods or the nanocubes. Furthermore, a significant shift of the G-band to higher frequency is observed following the laser irradiation of the GO solutions containing the Au nanorods or the nanocubes (1603 and 1601 cm^{-1}, respectively, compared to 1594 cm^{-1} in the absence of Au nanoparticles). This shift is consistent with doping graphene with electron acceptors, thus, the Au nanoparticles are acting as week electron acceptors that induce a charge transfer from graphene to the Au nanoparticles.[58] The increase in the D/G intensity ratio compared to the LCG (Figure 7A) and the blue shift of the G-band are taken as evidence for the presence of more structural defects in the graphene lattice induced by laser irradiation of GO in the presence of Au nanoparticles. These defect sites in the reduced GO nanosheets act as favorable nucleation sites for the ultrasmall Au nanoparticles that, by occupying these vacancies, are no longer mobile for the Ostwald ripening process to take place, thus, the formation of large Au nanoparticles and aggregates is significantly decreased.

CONCLUSIONS

In summary, the coupling of the surface plasmon resonance of gold nanoparticles with the laser reduction of graphene oxide leads to significant enhancement of the efficiency of photothermal energy conversion by the gold nanoparticles–graphene oxide mixtures. The enhanced photothermal effects can be tuned by controlling the shape and size of the gold nanostructures that result in a remarkable increase in the heating efficiency of the laser-induced melting and size reduction of gold nanostructures. The large surface areas of the laser reduced graphene oxide nanosheets with multiple defect sites and vacancies provide efficient nucleation sites for the ultrasmall gold nanoparticles to be anchored to the graphene surface. This defect filling mechanism decreases the mobility of the ultrasmall gold nanoparticles and, thus, stabilizes the particles against the Ostwald ripening process that leads to a broad size distribution of the laser-size-reduced gold nanoparticles. The ultrasmall gold–graphene nanocomposites are proposed as novel photothermal energy convertors for a variety of thermochemical and thermomechanical applications, in addition to photothermal therapy, such as heating and evaporation of liquids by solar energy, ignition of solid fuels, and welding of composite materials.

EXPERIMENTAL SECTION

Preparation of Graphene Oxide Nanosheets. In the experiments, GO was prepared by the oxidation of high purity graphite powder (99.9999%, 200 mesh, Alfa Aesar) according to the method of Hummers and Offeman.[59] After repeated washing of the resulting yellowish-brown cake with hot water, it was dried at room temperature under vacuum overnight. A total of 2 mg dried GO was sonicated in 10 mL of deionized water until a homogeneous yellow dispersion was obtained.

Preparation of Spherical Gold Nanoparticles. Spherical Au nanoparticles were prepared by the standard citrate reduction procedure, as described in the literature.[38] A total of 100 mL of 1 mM $HAuCl_4$ aqueous solution was heated until boiling, and then 10 mL of 38 mM trisodium citrate solution was added under continuous stirring for 15 min.

Preparation of Shape-Controlled Gold Nanostructures. Au nanostructures of different shapes were prepared utilizing the seed-mediated method,[32,33] with little modifications. First, the Au-seed solution was prepared by the addition of aqueous $NaBH_4$ (300 μL, 10^{-2} M) to a mixture of $HAuCl_4$ (2.5 mL, 5×10^{-4} M) and CTAB (2.5 mL, 2×10^{-1} M) at room temperature under vigorous stirring. For the synthesis of different shapes, 80 μL of the freshly prepared Au-seed solution was added to different growth solutions to initiate anisotropic growth of Au nanoparticles with different shapes. The different growth solutions contained the same $HAuCl_4$ and CTAB concentrations, but different amounts of $AgNO_3$, and were utilized to grow various morphologies, namely, spheroids, SRs, LRs, bipyramids, rounded-corner rectangles, sharp-corner rectangles, cubes, and dog bones. Each of the growth solutions was prepared by first mixing $HAuCl_4$ (25 mL, 10^{-3} M) and CTAB (25 mL, 2×10^{-1} M) solutions followed by the addition of 70 μL of ascorbic acid (78.8×10^{-3} M), which resulted in discoloration of the yellowish Au–CTAB mixture due to the partial reduction of Au ions. Then the designated amount of $AgNO_3$ was added to the colorless mixture followed by the subsequent addition of the seed to catalyze the growth. All growth solutions were kept undisturbed at a temperature of 25–28 °C for 2 h. The absorption spectra of different Au nanoparticles were recorded for the as-prepared fresh samples diluted in DI water. The final concentrations of $AgNO_3$ in the growth solutions required for the growth of different shapes are as follows: spheroids (4×10^{-7} M), SRs (8×10^{-7} M), LRs (8×10^{-6} M), bipyramids (12×10^{-6} M), rounded-corner rectangles (13×10^{-6} M), sharp-corner rectangles (14×10^{-6} M), cubes (16×10^{-6} M), and dog bones (32×10^{-6} M). All chemicals used were 99.99% purity as obtained from Sigma-Aldrich, U.S.A.

Laser Irradiation and Photothermal Measurements. For the laser irradiation and photothermal synthesis of ultrasmall Au–graphene nanocomposites, an aqueous dispersion of GO and preformed selected-shape Au nanoparticles was prepared by mixing 1 mL of Au-nanoparticles solution with 2 mL of GO solution (2 mg/10 mL), and the mixture was irradiated in a quartz cuvette with the unfocused beam of the second and third harmonics of a Nd:YAG laser (second harmonic $\lambda = 532$ nm, average power 4 W, $h\nu = 2.32$ eV, or third harmonic $\lambda = 355$ nm, average power 2 W, $h\nu = 3.49$ eV, pulse width $\tau = 7$ ns, repetition rate = 30 Hz, fluence ~ 0.1 J/cm^2, Spectra Physics LAB-170–30). The beam diameter was measured to be 7–9 mm for both the 532 and the 355 nm. The solutions were magnetically stirred during the irradiation. For the Au size reduction experiments in the absence of GO, 1 mL of the shape-selected Au-nanoparticles solution was irradiated under similar laser conditions as described above (irradiation for 10 min corresponding to 18000 laser shots). The temperature of the solution was monitored during irradiation using a thermocouple immersed in the solution.

Characterization Measurements. TEM images were obtained using a Joel JEM-1230 electron microscope operated at 120 kV equipped with a Gatan UltraScan 4000SP 4K × 4K CCD camera. Absorption spectra were recorded using a Hewlett-Packard HP-8453 diode array spectrophotometer. The Raman spectra were measured using an excitation wavelength of 457.9 nm provided by a Spectra-Physics model 2025 argon ion laser. The laser beam was focused to a 0.10 mm diameter spot on the sample with a laser

power of 3 mW. The samples were pressed into carbon tape supported on glass coverslip, held at a 30° angle in the path of the laser beam. The detector was a Princeton Instruments 1340 × 400 liquid nitrogen CCD detector, attached to a Spex model 1870 0.5 m single spectrograph with interchangeable 1200 and 600 lines/mm holographic gratings (Jobin-Yvon). The Raman scattered light was collected by a Canon 50 mm f/0.95 camera lens. Though the holographic gratings provided high discrimination, Schott and Corning glass cutoff filters were used to provide additional filtering of reflected laser light, when necessary.

Conflict of Interest: The authors declare no competing financial interest.

Acknowledgment. We thank the National Science Foundation (CHE-0911146) for the support of this work. We thank Natalie P. Herring (VCU) for the assistance with the TEM measurements.

Supporting Information Available: UV−vis absorption spectra and TEM images of the Au seed and the spherical Au nanoparticles and comparison between the absorption spectra and the TEM images of the laser-irradiated Au nanoparticles of different shapes in graphene oxide solutions are included. This material is available free of charge *via* the Internet at http://pubs.acs.org.

REFERENCES AND NOTES

1. Eustis, S.; El-Sayed, M. A. Why Gold Nanoparticles are More Precious than Pretty Gold: Noble Metal Surface Plasmon Resonance and Its Enhancement of the Radiative and Nonradiative Properties of Nanocrystals of Different Shapes. *Chem. Soc. Rev.* **2006**, *35*, 209–217.
2. Jain, P. K.; Huang, X. H.; El-Sayed, I. H.; El-Sayed, M. A. Noble Metals on the Nanoscale: Optical and Photothermal Properties and Some Applications in Imaging, Sensing, Biology, And Medicine. *Acc. Chem. Res.* **2008**, *41*, 1578–1586.
3. Murphy, C. J.; Thompson, L. B.; Alkilany, A. M.; Sisco, P. N.; Boulos, S. P.; Sivapalan, S. T.; Yang, J. A.; Chernak, D. J.; Huang, J. The Many Faces of Gold Nanorods. *J. Phys. Chem. Lett.* **2010**, *1*, 2867–2875.
4. Ringe, E.; Langille, M. R.; Sohn, K.; Zhang, J.; Huang, J.; Mirkin, C. A.; Van Duyne, R. P.; Marks, L. D. Plasmon Length: A Universal Parameter to Describe Size Effects in Gold Nanoparticles. *J. Phys. Chem. Lett.* **2012**, *3*, 1479–1483.
5. Link, S.; El-Sayed, M. A. Size and Temperature Dependence of the Plasmon Absorption of Colloidal Gold Nanoparticles. *J. Phys. Chem. B* **1999**, *103*, 4212–4217.
6. Chou, C.-H.; Chen, C.-D.; Wang, C. R. C. Highly Efficient, Wavelength-Tunable, Gold Nanoparticle Based Optothermal Nanoconvertors. *J. Phys. Chem. B* **2005**, *109*, 11135–11138.
7. Huang, X.; Jain, P. K.; El-Sayed, I. H.; El-Sayed, M. A. Plasmonic Photothermal Therapy (PPTT) Using Gold Nanoparticles. *Lasers Med. Sci* **2008**, *23*, 217–228.
8. Gobin, A. M.; Lee, M. H.; Halas, N. J.; James, W. D.; Drezek, R. A.; West, J. L. Near-Infrared Resonant Nanoshells for Combined Optical Imaging and Photothermal Cancer Therapy. *Nano Lett.* **2007**, *7*, 1929–1934.
9. Tong, L.; Wei, Q.; Wei, A.; Cheng, J.-X. Gold Nanorods as Contrast Agents for Biological Imaging: Optical Properties, Surface Conjugation and Photothermal Effects. *Photochem. Photobiol.* **2009**, *85*, 21.
10. Hirsch, L. R.; Stafford, R. J.; Bankson, J. A.; Sershen, S. R.; Rivera, B.; Rrice, R. E.; Hazle, J. D.; Halas, N. J.; West, J. L. Nanoshell-Mediated Near-Infrared Thermal Therapy of Tumors under Magnetic Resonance Guidance. *Proc. Natl. Acad. Sci. U.S.A.* **2003**, *100*, 13549–13554.
11. Zhang, J. Z. Biomedical Applications of Shape-Controlled Plasmonic Nanostructures: A Case Study of Hollow Gold Nanospheres for Photothermal Ablation Therapy of Cancer. *J. Phys. Chem. Lett.* **2010**, *1*, 686–695.
12. Kamat, P. V. Photophysical, Photochemical, and Photocatalytic Aspects of Metal Nanoparticles. *J. Phys. Chem. B* **2002**, *106*, 7729–7744.
13. Zhang, J. Z.; Schwartzberg, A. M.; Norman, T.; Grant, C. D.; Liu, J.; Bridges, F.; van Buuren, T. Comment on "Gold Nanoshells Improve Single Nanoparticle Molecular Sensors. *Nano Lett.* **2005**, *5*, 809–810.
14. Schwartzberg, A. M.; Zhang, J. Z. Novel Optical Properties and Emerging Applications of Metal Nanostructures. *J. Phys. Chem. C* **2008**, *112*, 10323–10337.
15. Kam, N. W. S.; O'Connell, M.; Wisdom, J. A.; Dai, H. Carbon Nanotubes as Multifunctional Biological Transporters and Near-Infrared Agents for Selective Cancer Cell Destruction. *Proc. Natl. Acad. Sci. U.S.A.* **2005**, *102*, 11600–11605.
16. Chakravarty, P.; Marches, R.; Zimmerman, N. S.; Swafford, A. D. E.; Bajaj, P.; Musselman, I. H.; Pantano, P.; Draper, R. K.; Vitetta, E. S. Thermal Ablation of Tumor Cells with Anti Body-Functionalized Single-Walled Carbon Nanotubes. *Proc. Natl. Acad. Sci. U.S.A.* **2008**, *105*, 8697–8702.
17. Zhou, F.; Xing, D.; Ou, Z.; Wu, B.; Resasco, D. E.; Chen, W. R. Cancer Photothermal Therapy in the Near-Infrared Region by Using Single-Walled Carbon Nanotubes. *J. Biomed. Opt.* **2009**, *14*, 021009.
18. Ghosh, S.; Dutta, S.; Gomes, E.; Carroll, D.; D'Agostino, R.; Olson, J.; Guthold, M.; Gmeiner, W. H. Increased Heating Efficiency and Selective Thermal Ablation of Malignant Tissue with DNA-Encased Multiwalled Carbon Nanotubes. *ACS Nano* **2009**, *3*, 2667.
19. Liu, Z.; Robinson, J. T.; Sun, X.; Dai, H. PEGylated Nano-Graphene Oxide for Delivery of Water Insoluble Cancer Drugs. *J. Am. Chem. Soc.* **2008**, *130*, 10876.
20. Yang, K.; Zhang, S.; Zhang, G.; Sun, X.; Lee, S.-T.; Liu, Z. Graphene in Mice: Ultrahigh *In Vivo* Tumor Uptake and Efficient Photothermal Therapy. *Nano Lett.* **2010**, *10*, 3318–3323.
21. Robinson, J. T.; Tabakman, S. M.; Liang, Y.; Wang, H.; Casalongue, H. S.; Vinh, D.; Dai, H. Ultrasmall Reduced Graphene Oxide with High Near-Infrared Absorbance for Photothermal Therapy. *J. Am. Chem. Soc.* **2011**, *133*, 6825–6831.
22. Geim, A. K.; Novoselov, K. S. The Rise of Graphene. *Nat. Mater.* **2007**, *6*, 183–191.
23. Rao, C. N. R.; Sood, A. K.; Subrahmanyam, K. S.; Govindaraj, A. Graphene: The New Two-Dimensional Nanomaterial. *Angew. Chem., Int. Ed* **2009**, *48*, 7752–7777.
24. Abdelsayed, V.; Moussa, S.; Hassan, H. M.; Aluri, H. S.; Collinson, M. M.; El-Shall, M. S. Photothermal Deoxygenation of Graphite Oxide with Laser Excitation in Solution and Graphene-Aided Increase in Water Temperature. *J. Phys. Chem. Lett.* **2010**, *1*, 2804–2809.
25. Moussa, S.; Atkinson, G.; El-Shall, M. S.; Shehata, A.; Abou-Zeid, K. M.; Mohamed, M. B. Laser Assisted Photocatalytic Reduction of Metal Ions by Graphene Oxide. *J. Mater. Chem.* **2011**, *21*, 9608–9619.
26. Takami, A.; Kurita, H.; Koda, S. Laser-Induced Size Reduction of Noble Metal Particles. *J. Phys. Chem. B* **1999**, *103*, 1226.
27. Inasawa, S.; Sugiyama, M.; Yamaguchi, Y. Bimodal Size Distribution of Gold Nanoparticles under Picosecond Laser Pulses. *J. Phys Chem. B* **2005**, *109*, 9404.
28. Yamada, K.; Tokumoto, Y.; Nagata, T.; Mafune, F. Mechanism of Laser-Induced Size-Reduction of Gold Nanoparticles As Studied by Nanosecond Transient Absorption Spectroscopy. *J. Phys. Chem. B* **2006**, *110*, 11751.
29. Muto, H.; Miyajima, K.; Mafune, F. Mechanism of Laser-Induced Size Reduction of Gold Nanoparticles As Studied by Single and Double Laser Pulse Excitation. *J. Phys. Chem. C* **2008**, *112*, 5810.
30. Pyatenko, A.; Yamaguchi, M.; Suzuki, M. Mechanisms of Size Reduction of Colloidal Silver and Gold Nanoparticles Irradiated by Nd:YAG Laser. *J. Phys. Chem. C* **2009**, *113*, 9078.
31. Werner, D.; Hashimoto, S.; Uwada, T. Remarkable Photothermal Effect of Interband Excitation on Nanosecond Laser-Induced Reshaping and Size Reduction of Pseudospherical Gold Nanoparticles in Aqueous Solution. *Langmuir* **2010**, *26*, 9956–9963.
32. Gole, A.; Murphy, C. J. Seed-Mediated Synthesis of Gold Nanorods: The Role of the Size and Nature of the Seed. *Chem. Mater.* **2004**, *16*, 3633–3640.

33. Sau, T. K.; Murphy, C. J. Seeded High Yield Synthesis of Short Au Nanorods in Aqueous Solution. *Langmuir* **2004**, *20*, 6414–6420.
34. Murphy, C. J.; Sau, T. K.; Gole, A. M.; Orendorff, C. J.; Gao, J. X.; Gou, L.; Hunyadi, S. E.; Li, T. Anisotropic Metal Nanoparticles: Synthesis, Assembly, and Optical Applications. *J. Phys. Chem. B* **2005**, *109*, 13857–13870.
35. Link, S.; Mohamed, M. B.; El-Sayed, M. A. Simulation of the Optical Absorption Spectra of Gold Nanorods as a Function of Their Aspect Ratio and the Effect of the Medium Dielectric Constant. *J. Phys. Chem. B* **1999**, *103*, 3073–3077.
36. Mohamed, M. B.; AbouZeid, K. M.; Abdelsayed, V.; Aljarash, A. A.; El-Shall, M. S. Growth Mechanism of Anisotropic Gold Nanocrystals *via* Microwave Synthesis: Formation of Dioleamide by Gold Nanocatalysis. *ACS Nano* **2010**, *4*, 2766.
37. Varnavski, O.; Ramakrishna, G.; Kim, J.; Lee, D.; Goodson, T., III Critical Size for the Observation of Quantum Confinement in Optically Excited Gold Clusters. *J. Am. Chem. Soc.* **2010**, *132*, 16–17.
38. Enüstün, B. V.; Turkevich, J. Coagulation of Colloidal Gold. *J. Am. Chem. Soc.* **1963**, *85*, 3317–3328.
39. Jin, L.; Yang, K.; Yao, K.; Zhang, S.; Tao, H.; Lee, S.-T.; Liu, Z.; Peng, R. Functionalized Graphene Oxide in Enzyme Engineering: A Selective Modulator for Enzyme Activity and Thermostability. *ACS Nano* **2012**, *6*, 4864–4875.
40. Ma, X.; Tao, H.; Yang, K.; Feng, L.; Cheng, L.; Shi, X.; Li, Y.; Guo, L.; Liu, Z. A Functionalized Graphene Oxide-Iron Oxide Nanocomposite for Magnetically Targeted Drug Delivery, Photothermal Therapy, and Magnetic Resonance Imaging. *Nano Res.* **2012**, *5*, 199–212.
41. Mu, Q.; Su, G.; Li, L.; Gilbertson, B. O.; Yu, L. H.; Zhang, Q.; Sun, Y.-P.; Yan, B. Size-Dependent Cell Uptake of Protein-Coated Graphene Oxide Nanosheets. *ACS Appl. Mater. Interfaces* **2012**, *4*, 2259–2266.
42. Zhou, X.; Zhang, Y.; Wang, C.; Wu, X.; Yang, Y.; Zheng, B.; Wu, H.; Guo, S.; Zhang, J. Photo-Fenton Reaction of Graphene Oxide: A New Strategy to Prepare Graphene Quantum Dots for DNA Cleavage. *ACS Nano* **2012**, *6*, 6592–6599.
43. Yang, K.; Hu, L.; Ma, X.; Ye, S.; Cheng, L.; Shi, X.; Li, C.; Li, Y.; Liu, Z. Multimodal Imaging Guided Photothermal Therapy Using Functionalized Graphene Nanosheets Anchored with Magnetic Nanoparticles. *Adv. Mater.* **2012**, *24*, 1868–1872.
44. Wang, X.; Wang, C.; Cheng, L.; Lee, S. T.; Liu, Z. Noble Metal Coated Single-Walled Carbon Nanotubes for Applications in Surface Enhanced Raman Scattering Imaging and Photothermal Therapy. *J. Am. Chem. Soc.* **2012**, *134*, 7414–7422.
45. Lee, Y. H.; Polavarapu, L.; Gao, N.; Yuan, P.; Xu, Q.-H. Enhanced Optical Properties of Graphene Oxide−Au Nanocrystal Composites. *Langmuir* **2011**, *28*, 321–326.
46. Ratke, L.; Voorhees, P. W. *Growth and Coarsening − Ostwald Ripening in Materials Processing*; Springer-Verlag: New York, 2002.
47. Meyer, J. C.; Kisielowski, C.; Erni, R.; Rossell, M. D.; Crommie, M. F.; Zettl, A. Direct Imaging of Lattice Atoms and Topological Defects in Graphene Membranes. *Nano Lett.* **2008**, *8*, 3582–3586.
48. Girit, C. O.; Meyer, J. C.; Erni, R.; Rossell, M. D.; Kisielowski, C.; Yang, L.; Park, C.-H.; Crommie, M. F.; Cohen, M. L.; Louie, S. G.; et al. Graphene at the Edge: Stability and Dynamics. *Science* **2009**, *323*, 1705–1708.
49. Bagri, A.; Mattevi, C.; Acik, M.; Chabal, Y. J.; Chhowalla, M.; Shenoy, V. B. Structural Evolution during the Reduction of Chemically Derived Graphene Oxide. *Nat. Chem.* **2010**, *2*, 581–587.
50. Gómez-Navarro, C.; Meyer, J. C.; Sundaram, R. S.; Chuvilin, A.; Kurasch, S.; M. Burghard, M.; Kern, K.; Kaiser, U. Atomic Structure of Reduced Graphene Oxide. *Nano Lett.* **2010**, *10*, 1144–1148.
51. Banhart, F.; Kotakoski, J.; Krashennnikov, A. V. Structural Defects in Graphene. *ACS Nano* **2011**, *5*, 26–41.
52. Kim, G.; Jhi, S.-H. Carbon Monoxide-Tolerant Platinum Nanoparticle Catalysts on Defect-Engineered Graphene. *ACS Nano* **2011**, *5*, 805.
53. Matsumoto, Y.; Koinuma, M.; Ida, S.; Hayami, S.; Taniguchi, T.; Hatakeyama, K.; Tateishi, H.; Watanabe, Y.; Amano, S. Photoreaction of Graphene Oxide Nanosheets in Water. *J. Phys. Chem. C* **2011**, *115*, 19280–19286.
54. Moussa, S.; Siamaki, A. R.; Gupton, B. F.; El-Shall, M. S. Pd-Partially Reduced Graphene Oxide Catalysts (Pd/PRGO): Laser Synthesis of Pd Nanoparticles Supported on PRGO Nanosheets for Carbon−Carbon Cross Coupling Reactions. *ACS Catal.* **2012**, *2*, 145–154.
55. Ferrari, A. C. Raman Spectroscopy of Graphene and Graphite: Disorder, Electron-Phonon Coupling, Doping and Nonadiabatic Effects. *Solid State Commun.* **2007**, *446*, 60.
56. Berciaud, S.; Ryu, S.; Brus, L. E.; Heinz, T. F. Graphene Oxidation: Thickness Dependent Etching and Strong Chemical Doping. *Nano Lett.* **2008**, *8*, 1965.
57. Cancado, L. G.; Jorio, A.; Martins Ferreira, E. H.; Stavale, F.; Achete, C. A.; Capaz, R. B.; Moutinho, M. V. O.; Lombardo, A.; Kulmala, T. S.; Ferrari, A. C. Quantifying Defects in Graphene *via* Raman Spectroscopy at Different Excitation Energies. *Nano Lett.* **2011**, *11*, 3190–3196.
58. Subrahmanyam, K. S.; Manna, A. K.; Pati, S. K.; Rao, C. N. R. A Study of Graphene Decorated with Metal Nanoparticles. *Chem. Phys. Lett.* **2010**, *497*, 70–75.
59. Hummers, W. S., Jr.; Offeman, R. E. Preparation of Graphitic Oxide. *J. Am. Chem. Soc.* **1958**, *80*, 1339–1339.